JOURNAL OF APPLIED CRYSTALLOGRAPHY

ISSN: 1600-5767
journals.iucr.org/j

Determination of the melting temperature of spherical nanoparticles in dilute solution as a function of their radius by exclusively using the small-angle X-ray scattering technique

Guinther Kellermann, Felipe L. C. Pereira and Aldo F. Craievich

J. Appl. Cryst. (2020). **53**, 455–463

JOURNAL OF APPLIED CRYSTALLOGRAPHY
ISSN 1600-5767

Determination of the melting temperature of spherical nanoparticles in dilute solution as a function of their radius by exclusively using the small-angle X-ray scattering technique

Guinther Kellermann,[a]* Felipe L. C. Pereira[a] and Aldo F. Craievich[b]

[a]Department of Physics, University Federal of Paraná, Curitiba, Brazil, and [b]Institute of Physics, University of São Paulo SP, São Paulo, Brazil. *Correspondence e-mail: keller@fisica.ufpr.br

Received 6 December 2019
Accepted 14 February 2020

Edited by V. Holý, Charles University, Prague, Czech Republic and CEITEC at Masaryk University, Brno, Czech Republic

Keywords: small-angle X-ray scattering; SAXS; melting; nanoparticles; thermal expansion; size-dependent contraction.

In this investigation the dependence on radius of the melting temperature of dilute sets of spherical nanocrystals with wide radius distributions was determined by a novel procedure exclusively using the results of small-angle X-ray scattering (SAXS) measurements. This procedure is based on the sensitivity of the SAXS function to small and rather sharp variations in the size and electron density of nanocrystals at their melting temperature. The input for this procedure is a set of experimental SAXS intensity functions at selected q values for varying sample temperatures. In practice, the sample is heated from a minimum temperature, lower than the melting temperature of the smallest nanocrystals, up to a temperature higher than the melting temperature of the largest nanocrystals. The SAXS intensity is recorded *in situ* at different temperatures during the heating process. This novel procedure was applied to three samples composed of dilute sets of spherical Bi nanocrystals with wide radius distributions embedded in a sodium borate glass. The function relating the melting temperature of Bi nanocrystals with their radius – determined by using the procedure proposed here – agrees very well with the results reported in previous experimental studies using different methods. The results reported here also evidence the predicted size-dependent contraction of Bi nanocrystals induced by the large surface-to-volume ratio of small nanocrystals and an additional size-independent compressive stress caused by the solid glass matrix in which liquid Bi nanodroplets are initially formed. This last effect is a consequence of the increase in the volume of Bi nanoparticles upon crystallization and also of differences in the thermal expansion coefficients of the crystalline phase of Bi and the glass matrix. This additional stress leads to a depression of about 10 K in the melting temperature of the Bi nanocrystals confined in the glass. The procedure described here also allowed the determination of the specific masses and thermal expansion coefficients of Bi nanoparticles in both liquid and crystalline phases.

1. Introduction

The thermal stability of small crystallites in the nanometric size range has been an important research issue in recent decades. Therefore, the search for experimental procedures providing accurate characterization of different properties of nanocrystals, such as the size dependence of their melting temperature, has attracted the attention of many researchers (Liu & Wang, 2015; Li *et al.*, 2017). The melting temperature of nanocrystals is strongly influenced by their surface energy, or by their interface energy in the case of nanocrystals embedded in matrices or supported on substrates. This leads to melting temperatures that can be much lower or sometimes higher than the melting temperature of the same bulk material with

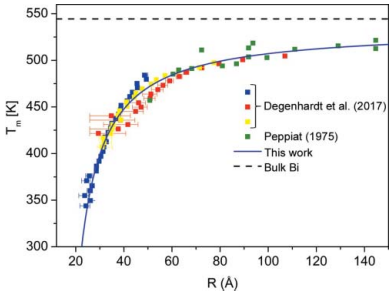

macroscopic size (Mei & Lu, 2007). Another reported effect related to nanocrystals is the decrease in lattice parameters as compared to the lattice parameters of the bulk crystals (Mays *et al.*, 1968; Wasserman & Vermaak, 1972; Muller *et al.*, 1987; Yu *et al.*, 1999; Jiang *et al.*, 2001; Liang *et al.*, 2003). Both size-dependent melting temperature and lattice contraction are consequences of the large fraction of atoms on the surface of small nanocrystals having coordination numbers much smaller than those of the atoms inside the nanoparticle.

In order to investigate the size dependence of the melting temperatures of nanocrystals, many experimental techniques have been used, namely differential thermal analysis and differential scanning calorimetry (Dick *et al.*, 2002; Sheng *et al.*, 1997; Lavčević & Ogorelec, 2003; Jo *et al.*, 2011), optical reflection and transmission (Garrigos *et al.*, 1986; Haro-Poniatowski *et al.*, 2005), transmission electron microscopy (Xu *et al.*, 2007; Goldstein *et al.*, 1992), and X-ray diffraction (Wang & Zhu, 2015; Freitas *et al.*, 2006). Although these techniques generally provide useful results, they may in some cases be subject to severe drawbacks. For example, for samples containing spherical nanoparticles exhibiting a wide radius dispersion, thermal analyses, optical measurements and X-ray diffraction techniques only allow one to determine their melting temperature as a function of their average radius. Since nanocrystals of different sizes melt at different temperatures, in the cases of samples with a wide size distribution, these procedures usually lead to poor results.

On the other hand, electron microscopy techniques can be used to determine the melting temperature of individual nanocrystals by examining changes in shape of faceted crystallites or by analyzing electron diffraction patterns. However, this procedure is very time consuming because it requires many observations of melting transitions in a high number of individual nanocrystals.

Obviously, X-ray and electron diffraction techniques are very sensitive to the nature of the atomic arrangement and thus well suited for the characterization of transitions from crystalline to liquid phases. However, for samples composed of randomly oriented nanocrystals, X-ray diffraction only probes the small fraction of crystallites that are oriented satisfying Bragg's law. In the case of a dilute set of nanocrystals this may be a serious drawback.

Other challenges regarding the determination of melting temperature relate to nanoparticles with amorphous or vitreous structure. Since the atomic arrangement of amorphous solids does not significantly differ from that of its melted phase, the X-ray diffraction technique does not usually provide useful results. Another experimental procedure that uses results of simultaneous measurements of wide-angle X-ray diffraction and small-angle X-ray scattering (SAXS) has been proposed and applied in previous work (Kellermann & Craievich, 2002; Kellermann & Craievich, 2008; Degenhardt *et al.*, 2017). By using this procedure the radius dependence of the melting temperature $T_m(R)$ function was determined for samples composed of diluted solutions of spherical Bi nanocrystals with a wide radius distribution embedded in a glass matrix.

In the present work we propose a novel experimental procedure for the determination of the radius dependence of the melting temperature of dilute sets of spherical nanoparticles – with a wide radius distribution – by measuring exclusively SAXS intensity curves at varying temperatures. This method is based on the sensitivity of the SAXS method to the small but rather sharp variation in size and electron density of nanocrystals at their melting transition. Differently from wide-angle X-ray diffraction, the SAXS technique has the advantage of probing all nanocrystals (irrespective of their orientations), thus leading to a much higher scattering intensity and therefore improving the accuracy of the derived results. In addition, *in situ* SAXS studies allow one to characterize changes in the size of nanoparticles held at various temperatures, thus allowing for the determination of the volumetric coefficients of thermal expansion of crystalline, amorphous or liquid nanoparticles embedded in solid matrices.

The proposed procedure was applied to the determination of the melting temperature T_m of spherical Bi nanocrystals, in dilute solution, embedded in a sodium borate glass as a function of their radius R. In order to determine the $T_m(R)$ functions over a wide radius range, three samples with wide radius distributions and different average radii were studied, thus covering a radius range from about 10 Å up to *ca* 110 Å. SAXS measurements as a function of temperature were performed *in situ* during the heating of glass samples containing Bi nanocrystals from room temperature up to temperatures above which all nanocrystals – with different sizes – are melted.

2. Theoretical background

2.1. Dependence of SAXS intensity on temperature

For free-standing nanocrystals or in the case in which nanoparticles are confined in a matrix with weak interaction between atoms on their surface and atoms of the matrix – not forming chemical bonds – the melting temperature decreases with decreasing nanocrystal radius. In this case, the SAXS intensity of a diluted set of spherical nanoparticles as a function of temperature is given by

$$I(q,T) = \int_{R_{\min}}^{R_m(T)} \left|F_l\left[R_l(T),q\right]\right|^2 N\left[R(T_0)\right] \mathrm{d}R + \int_{R_m(T)}^{\infty} \left|F_c\left[R_c(T),q\right]\right|^2 N\left[R(T_0)\right] \mathrm{d}R, \quad (1)$$

where $F[R(T),q]$ is the form factor scattering amplitude of a homogeneous spherical particle with a radius R, to be specified below, and $N[R(T_0)]\,\mathrm{d}R$ is the radius distribution function defined as the number of nanoparticles having their radius value between R and $R+\mathrm{d}R$, T_0 is the temperature at which the $N[R(T_0)]$ function is determined, and $R_m(T)$ is the radius of the nanoparticles that melt at temperature T. The subscripts l and c refer to liquid and crystalline states, respectively. The variable q is the modulus of the scattering vector given by

$q = 4\pi \sin\theta/\lambda$, where θ is half the scattering angle and λ the X-ray wavelength.

Defining the function $\phi(qR)$ as

$$\phi(qR) = 3\frac{\sin qR - qR\cos qR}{qR^3}, \tag{2}$$

the scattering amplitude of a melted (liquid) nanoparticle with radius R_l, $F_l[R_l(T), q]$, and the scattering amplitude of a crystalline nanoparticle with radius R_c, $F_c[R_c(T), q]$, are given by

$$F_l\big[R_l(T), q\big] = \frac{4\pi}{3}\big[R_l(T)\big]^3\big[\rho_{el}(T, R_l) - \rho_{eg}(T)\big]\phi\big[qR_l(T)\big] \tag{3}$$

and

$$F_c\big[R_c(T), q\big] = \frac{4\pi}{3}\big[R_c(T)\big]^3\big[\rho_{ec}(T, R_c) - \rho_{eg}(T)\big]\phi\big[qR_c(T)\big], \tag{4}$$

respectively. In equations (3) and (4), ρ_{el} and ρ_{ec} are the electron densities of the liquid and crystalline phases, respectively, and ρ_{eg} the electron density of the matrix in which the nanoparticles are embedded.

In addition to the expected dependence on temperature associated with thermal expansion, the specific mass and thus the electron density of nanoparticles are also functions of their radius. As will be discussed in detail in the next section, this effect is a consequence of differences in the surface-to-volume ratio that induce different contraction effects, so the electron densities of small nanoparticles are higher than the densities of those with large sizes.

The radius of a nanoparticle after melting R_l and the radius R_c just before melting are simply related by

$$R_l = R_c(\rho_c/\rho_l)^{1/3}, \tag{5}$$

where ρ_c and ρ_l are the specific masses of the crystalline and liquid phases, respectively.

2.2. Lattice contraction and electron density as functions of temperature and nanoparticle radius

In order to calculate the SAXS intensity using equations (1)–(5), the values of the electron densities of nanoparticles at all temperatures and in both crystalline and liquid states are required. As a consequence of thermal expansion, the volume of nanoparticles increases on heating and thus ρ_{ec} and ρ_{el} decrease for increasing temperatures. Another effect on the electron density and specific mass of nanoparticles comes from the intrinsic size-dependent stress resulting from the larger surface-to-volume ratio of smaller nanoparticles (Jiang *et al.*, 2001). For nanoparticles with free surfaces – and for nanoparticles embedded in a matrix with weak interactions between surface and surrounding atoms – the inward attractive forces on the surface atoms produced by atoms inside the nanoparticle result in a compressive stress and therefore in a decrease in nanoparticle volume. The magnitude of this stress increases for decreasing nanoparticle radius, thus leading to an increase in the electron density and specific mass of the nanoparticles for decreasing nanoparticle size.

In analogy with the contraction of the lattice parameter in a crystalline structure, the relative contraction of a spherical particle ϵ is defined as

$$\epsilon = \frac{\Delta R}{R} = \frac{R - R_0}{R_0}, \tag{6}$$

where R_0 and R are the radius before and after the contraction, respectively. In terms of the relative change of its volume, $\Delta V/V_0$, or alternatively from the relative change in the specific mass, $\Delta\rho/\rho_0$, the contraction for small values of stress is given by

$$\epsilon = \frac{\Delta V}{3V_0} = \frac{-\Delta\rho}{3\rho_0}. \tag{7}$$

Here, $\Delta V/V_0 = (V - V_0)/V_0$ and $\Delta\rho/\rho_0 = (\rho - \rho_0)/\rho_0$, V_0 and ρ_0 being the volume and specific mass, respectively, of the non-contracted sphere and V and ρ being the volume and specific mass, respectively, which are different from V_0 and ρ_0 as a consequence of the size-dependent stress. In practice V_0 and ρ_0 are the values inside the bulk phases for which no size-dependent contraction is expected.

According to the Laplace–Young equation the pressure on a spherical nanoparticle of radius R is given by

$$P = 2f/R, \tag{8}$$

where f is the surface stress denoting the reversible work per unit area due to elastic strain.

Combining equation (8) with the definition of compressibility, $\kappa = -\Delta V/(V_0 P)$, we have

$$\frac{\Delta V}{V_0} = -\frac{2\kappa f}{R}. \tag{9}$$

Using equation (9) in the first equality of equation (7) gives the result that the size-dependent relative contraction of spherical nanocrystals, ϵ_c, having radius R can be determined from the relation

$$\epsilon_c = -\frac{2\kappa_c f_c}{3R}, \tag{10}$$

where κ_c and f_c are the compressibility and surface stress, respectively, of the bulk crystal.

Liang *et al.* (2003) showed that the surface stress on nanocrystals is given by

$$f_c = \left(\frac{3\gamma_{sl}h}{4\kappa_c}\right)^{1/2}, \tag{11}$$

where h is the atomic diameter and γ_{sl} is the solid/liquid free-energy excess per unit surface area corresponding to the reversible work per unit area to build up a new solid surface. A relation for γ_{sl} derived from the Gibbs–Thompson equation can be written as (Liang *et al.*, 2003)

$$\gamma_{sl} = \frac{2hS_{vib}H_m}{3V_{mol}\mathcal{R}}, \tag{12}$$

where S_{vib} is the vibrational part of the overall melting entropy, H_m and V_{mol} are the melting enthalpy and molar volume, respectively, of the bulk crystal, and $\mathcal{R}$ is the ideal gas constant. For a liquid nanoparticle with a free surface the surface stress is simply given by (Vanfleet & Mochel, 1995)

$$f_l = \gamma_{vl}, \tag{13}$$

where γ_{vl} is the specific vapor/liquid surface-free-energy excess. Combining equation (13) with equations (7), (8) and (9), the size-dependent relative contraction acting on spherical liquid droplets, ϵ_l, becomes

$$\epsilon_l = -\frac{2\kappa_l\gamma_{vl}}{3R}, \tag{14}$$

where κ_l is the compressibility of the liquid bulk phase.

From equation (7) it follows that the specific mass of crystalline and liquid nanoparticles is determined from the relation

$$\rho(T) = \rho_0(T)(1 - 3\epsilon), \tag{15}$$

where $\rho_0(T)$ is the specific mass of the bulk particle at temperature T. The value of ρ_0 at temperature T is calculated from the known value of ρ_0 at a given temperature T_0 using the relation

$$\rho_0(T) = \rho_0(T_0)\big[1 - \beta(T - T_0)\big], \tag{16}$$

where β is the coefficient of volume expansion. Finally, the electron density is calculated using the relation

$$\rho_e(T) = \frac{\sum f_i A Z_i}{M}\rho(T), \tag{17}$$

where Z_i and f_i are the atomic number and the fraction of atoms of the element i in the compound, respectively, A is the Avogadro number, and M is the molecular mass. For a single-element compound it is simply given by $\rho_e(T) = Z\rho(T)/M$.

Equations (15), (16) and (17) apply either to crystalline or to liquid nanoparticles. Therefore, the different parameters ρ, ρ_0, ϵ, β and ρ_e appearing in the pertinent equations should be those specifically referring to crystalline or to liquid phases. Notice that all these parameters in the liquid phase are different from those in the crystalline phase.

2.3. Dependence on radius of the melting temperature

Several theoretical models have being proposed for describing the radius dependence of the melting temperature of spherical nanoparticles (Wronski, 1967; Couchman & Jesser, 1977; Thomson, 1988; Kofman *et al.*, 1990; Shi, 1994; Vanfleet & Mochel, 1995; Jiang *et al.*, 2000). The most successful analytical function that describes the radius dependence of the melting temperature of nanocrystals was proposed by Shi (1994). Shi (1994) determined the melting temperature in terms of the vibrational part of the melting entropy, S_{vib}, derived from Mott's model, as follows:

$$T_m(R) = T_{mb}\exp\left[-\frac{(2S_{vib})/(3\mathcal{R})}{R/R_0 - 1}\right], \tag{18}$$

where T_{mb} is the melting temperature of the bulk crystal and $R_0 = 3h$ is the value of the radius of the nanocrystal for which all atoms are located on its surface.

3. Experimental

Glass samples containing dispersed Bi atoms were prepared using the conventional melt-quenching technique. B_2O_3 and Na_2CO_3 were used as raw materials for glass formation, and Bi_2O_3 was considered as a source of Bi atoms. SnO was added to partially reduce the bismuth oxide. All reagents were very finely ground in an agate mortar and mixed before melting. Small batches of about 7 g were melted in a vacuum atmosphere ($\sim 10^{-1}$ mbar; 1 mbar = 100 Pa) at 1318 K for a period of 1 h. The melt was then fast quenched down to room temperature using a splat-cooling device. Fast quenching inhibits the formation of Bi nanoparticles during the cooling process as well as avoiding the crystallization of the glass. As a result, thin Bi-containing glass plates transparent to visible light with a thickness in the 100–200 µm range were obtained. The composition of the glass samples inferred from the amount of each reagent used in the preparation is $28Na_2O$–$72B_2O_3$–$3SnO_2$–2Bi (mol%).

In order to promote the formation and growth of Bi nanoparticles with different wide radius distributions, three samples containing Bi atoms homogeneously dispersed in the glass were submitted to different isothermal treatments in the 813–838 K range. Since the temperatures in this range are higher than the melting temperature of bulk Bi, all Bi nanoparticles are in the liquid state during their growth. After the thermal treatment the samples were slowly cooled to room temperature, thus allowing the crystallization of the Bi nanodroplets. Previous X-ray diffraction studies of Bi nanoparticles of the same nanocomposite demonstrated that after cooling Bi nanoparticles crystallize in the same rhombohedral structure as bulk Bi (Kellermann & Craievich, 2002, 2008; Degenhardt *et al.*, 2017). Transmission electron microscopy images showed that nanocrystalline Bi particles have nearly spherical shape and some radius dispersion (Kellermann & Craievich, 2003).

The SAXS intensity functions of the studied samples were determined *in situ* during the heating of the samples from room temperature up to 620 K, this temperature being much higher than the melting temperature of all nanocrystals embedded in the glass. On the other hand, these temperatures are much lower than the temperatures required for appreciable diffusion of Bi in glass. Therefore, further growth of Bi nanoparticles during heating from room temperature up to 620 K could be safely neglected. These temperatures are also lower than the softening temperature of the glass matrix ($\sim$880 K). This implies that the glass plates remained solid over the whole temperature range over which Bi nanocrystals with different sizes have melted.

SAXS measurements were performed at the SAXS2 beamline of the Brazilian Synchrotron Laboratory (LNLS) using 1.5498 Å X-ray wavelength. A specially designed chamber was used for precise control of the sample

temperature during SAXS experiments (Kellermann *et al.*, 2003). The samples were maintained in vacuum at $\sim 10^{-1}$ mbar and heated in steps of 5 K, keeping a constant temperature during SAXS measurements. SAXS intensity patterns were recorded using a Mar165 2D CCD detector. Two scintillation detectors were used for recording the intensity of primary and transmitted X-ray beams, thus allowing for determination of sample transmission and varying intensity of the primary beam. The parasitic scattering intensity (from slits, air gaps and windows) was subtracted from the total SAXS intensity. Since the SAXS intensity produced by spherical particles in dilute solution is isotropic, the 2D SAXS intensity patterns were radially integrated, thus leading to the 1D q-dependent function of the SAXS intensity. Because of the very small cross section of the primary beam, the use of mathematical desmearing of SAXS curves was not required.

4. Results and discussion

4.1. Determination of the radius distribution function

Bi nanocrystals were grown in the three studied samples (labeled A, B and C) by submitting initially homogeneous glass precursors to the different isothermal treatments reported in Table 1. The experimental SAXS intensity curves corresponding to the three dilute solid solutions of spherical Bi nanoparticles embedded in a homogeneous sodium borate glass – measured at 297 K – are plotted in Fig. 1(*a*) (blue symbols). As *a priori* expected, a visual examination of the SAXS curves plotted in Fig. 1(*a*) suggests that the average sizes of the nanocrystals contained in each studied sample are clearly different.

For the determination of the radius distribution functions $N[R(T_0)]$ of the three studied samples at $T_0 = 297$ K, all Bi nanoparticles were assumed to be in the crystalline state. Under this assumption, the SAXS intensity would be given only by the second integral of equation (1). As will be shown later in our analysis, the temperature $T_0 = 297$ K is high enough to melt Bi nanocrystals having a radius smaller than 22 Å. However, the effect of this on the $N[R(T_0)]$ functions over the low-R limits is expected to be negligible because the variation in nanoparticle radius of Bi nanoparticles on melting is much smaller than their radii. Thus, in our investigation, the shapes of the $N[R(T_0)]$ functions determined from the procedure proposed here were considered as good approximations. On the other hand, the dependence on size and temperature of the electron density of the nanocrystals was determined using equations given in Section 2.2, which account for the intrinsic size-dependent stress and thermal expansion. Gaussian functions were assumed to describe the shape of the $N[R(T_0)]$ functions well.

Calculated SAXS curves determined from the best-fitting procedure are plotted as solid lines in Fig. 1(*a*). These results indicate that the calculated SAXS curves agree very well with the experimental curves (blue symbols). Fig. 1(*b*) shows the radius distribution functions corresponding to all studied samples determined from the best-fitting procedure. The partial overlapping of the three $N[R(T_0)]$ functions indicates that the analyses of our SAXS results allow us to probe Bi nanoparticles with a wide radius range, from about 10 Å up to *ca* 110 Å. The average radius and radius dispersion at 297 K derived from our best-fit analyses are reported in Table 1.

Table 1
Average radius $\langle R \rangle$ and radius dispersion σ (standard deviation) of polydisperse sets of Bi nanocrystals embedded in the sodium borate glass determined from best fitting of equation (1) to experimental SAXS curves recorded at 297 K.

The temperature and time periods of isothermal treatments for the processes of formation and growth of Bi nanoparticles in glass are also reported.

Sample	Thermal treatment	$\langle R \rangle$ (Å)	σ (Å)
A	823 K – 1 h	24.6	5.17
B	818 K – 20 min	43.4	11.07
C	838 K – 20 min	64.6	16.86

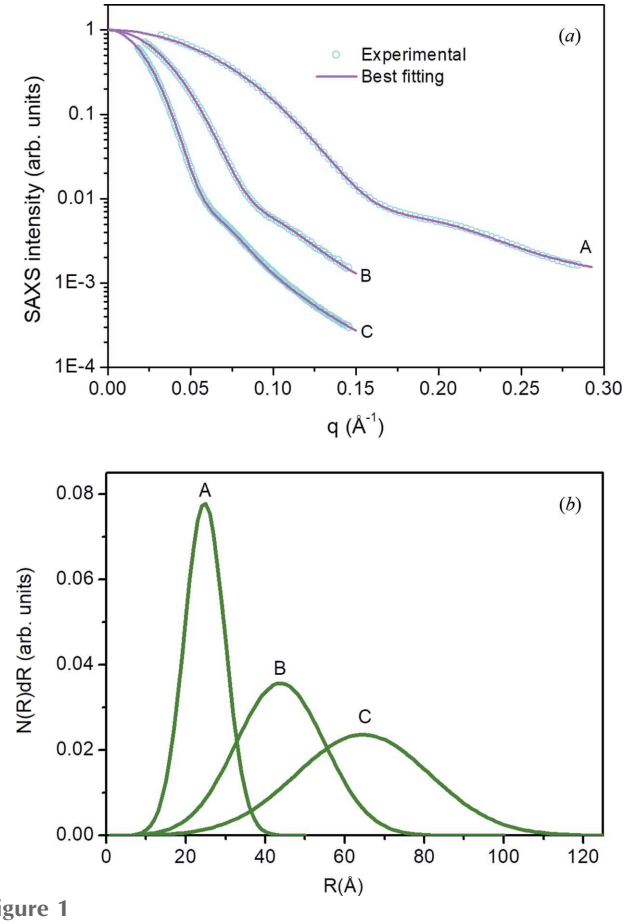

Figure 1
(*a*) Experimental SAXS intensity functions (blue symbols), measured at 297 K, produced by samples A, B and C, which contain spherical Bi nanocrystals embedded in Bi_2O_3 glass with different radius distributions. The solid lines are the SAXS curves calculated by the best-fitting procedure. The SAXS intensity curves were all normalized to unity at q = 0. (*b*) Radius distribution functions $N(R)$ determined from the best-fitting procedure with their integrals normalized to unity. Samples A, B and C are composed of polydisperse sets of Bi nanocrystals with different average radius, namely 24.6, 43.4 and 64.6 Å, respectively.

4.2. SAXS intensity as function of temperature

Fig. 2 shows the SAXS intensity as a function of temperature for several selected q values (blue symbols) corresponding to samples A, B and C, which contain polydisperse sets of Bi nanoparticles with different average radii and radius dispersions (see Table 1). The SAXS intensity curves displayed in Fig. 2 exhibit different temperature dependences over different temperature ranges, which for increasing temperatures correspond to the successive presences of only nanocrystals [range (i)], a mixture of nanocrystals and liquid nanodroplets [range (ii)], and only liquid nanodroplets [range (iii)], as described below.

(i) A low-temperature range is apparent in Figs. 2(*b*) and 2(*c*) below the temperatures at which Bi nanocrystals start to melt ($T < 450$ K for sample B and $T < 480$ K for sample C), in which the SAXS intensity exhibits a decreasing trend. This intensity decrease is a consequence of the thermal expansion of Bi nanocrystals for increasing temperatures.

(ii) An intermediate-temperature range is also apparent in Figs. 2(*b*) and 2(*c*), over which nanocrystals with increasing radius exhibit the crystal-to-liquid transition (450–500 K for sample B and 470–510 K for sample C). Over this range, a pronounced increase in the scattering intensity occurs. This increase in SAXS intensity is a consequence of the increase in electron density of Bi nanocrystals upon melting. Over this temperature range the melting of nanocrystals with different sizes occurs. The same temperature dependence is also observed for sample A [Fig. 2(*a*)] over a broader temperature range (297–450 K). Within the intermediate temperature range, both crystalline and liquid Bi nanoparticles coexist.

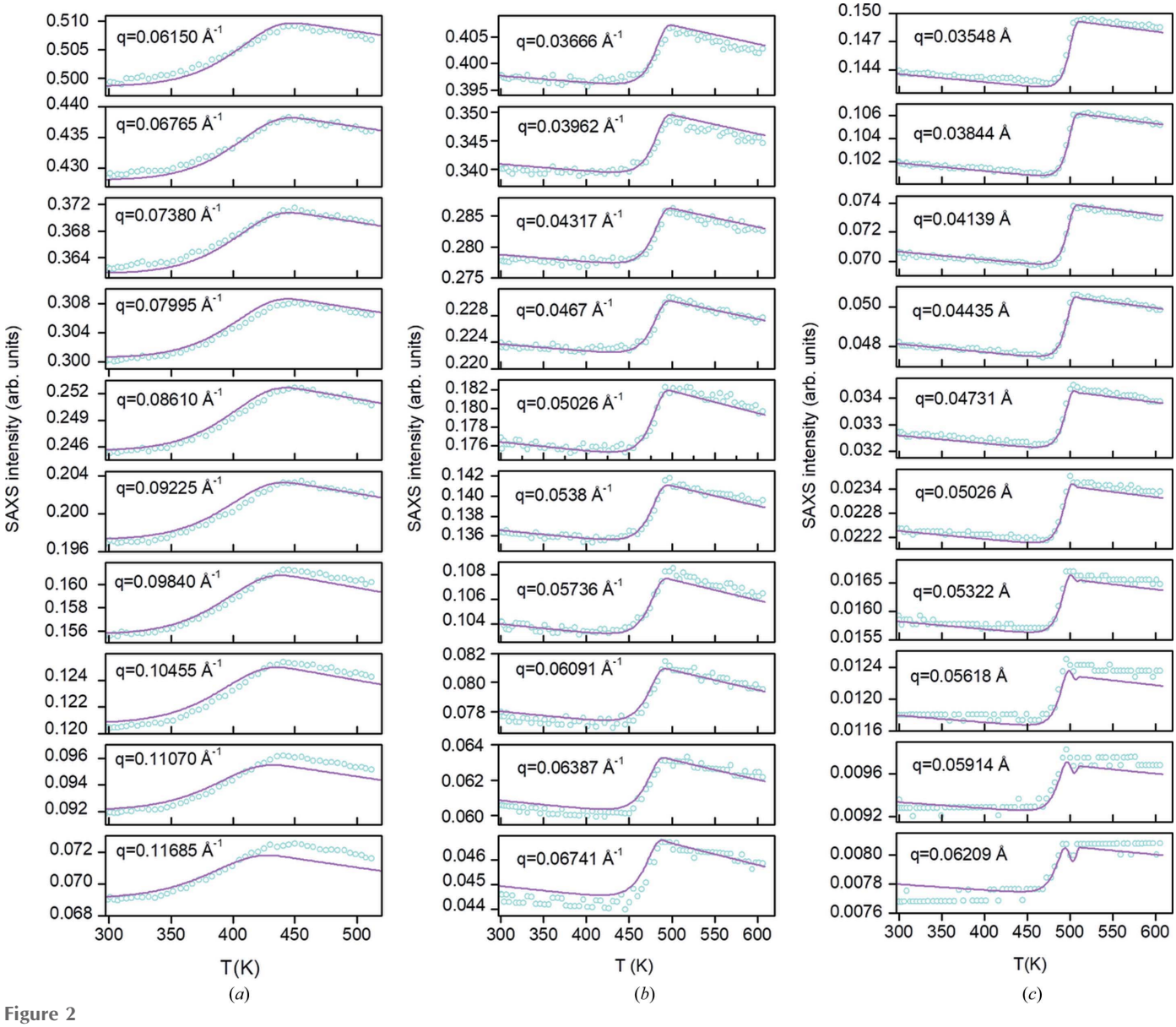

Figure 2
Experimental SAXS intensity as a function of temperature from three sets of Bi nanocrystals embedded in glass for the indicated values of the modulus of the scattering vector (blue symbols). The solid lines are the calculated curves assuming the model described in the text. Plots in columns (*a*), (*b*) and (*c*) show the temperature dependence of SAXS intensity curves corresponding to samples A, B and C, respectively.

Table 2
Values of different relevant parameters corresponding to crystalline and liquid phases of bulk Bi and sodium borate glass.

See the text for parameter definitions.

Parameter	Value	Reference
$\rho_{0\ \text{liquid Bi}}$ (kg m^{-3}) at 544.52 K	10050	Lide (1997)
$\rho_{0\ \text{crystal Bi}}$ (kg m^{-3}) at 293 K	9747	Emsley (1991)
$\rho_{0\ \text{glass}}$ (kg m^{-3}) at 297 K	2.40×10^{3}	This work
$\beta_{\text{liquid Bi}}$ (K^{-1})	1.21×10^{-4}	Sobolev (2010)
$\beta_{\text{crystal Bi}}$ (K^{-1})	4.02×10^{-5}	Lide (1997)
β_{glass} (K^{-1})	3.1×10^{-5}	Bobkova (2003)
$\kappa_{\text{liquid Bi}}$ (Pa^{-1})	3.64×10^{-11}	Sobolev (2010)
$\kappa_{\text{crystal Bi}}$ (Pa^{-1})	3.17×10^{-11}	Kittel (2005)
S_{vib} (J mol^{-1} K^{-1})	3.78	Regel & Glazov (1995)
H_{m} (J mol^{-1})	11.145×10^{3}	Archer (2004)
V_{mol} (m^{3}) crystal phase at 297 K	21.368×10^{-6}	Lide (1997)
γ_{vl} (J m^{2})	0.388	Aqra & Ayyad (2011)
$AZ_{\text{Bi}}/M_{\text{Bi}}$ (electrons g^{-1})	2.3918×10^{23}	–
$(\sum f_i AZ_i)/M_{\text{glass}}$ (electrons g^{-1})	2.8869×10^{23}	–

(iii) A high-temperature range can be seen in Figs. 2(*a*), 2(*b*) and 2(*c*), over which all nanoparticles are in the liquid state ($T > 450$ K for sample A, $T > 500$ K for sample B and $T > 510$ K for sample C). For all selected q values the $I(q)$ versus T curves exhibit a nearly linear behavior with a negative slope. The decrease in SAXS intensity over this high-temperature range is a consequence of the decrease in specific mass and electron density of liquid Bi droplets due to thermal expansion.

Regarding the behavior of the $I(q)$ versus T curves, note that in the case of Bi (as well as for Ge and Sb, for example) an increase in the specific mass occurs upon melting. The increase in the electron density of these nanoparticles embedded in glass – with electron densities lower than the electron density of the bulk material – would also result in an increase in SAXS intensity upon melting. On the other hand, for most metals, the specific mass decreases on melting; thus, in these cases, a decrease in SAXS intensity upon melting would be expected (Kellermann *et al.*, 2015).

The same procedure for the determination of the $N(R, T)$ function for samples held at $T = 297$ K can, in principle, be also applied to calculate the SAXS intensity $I(q, T)$ at any other temperature. However, for this purpose, additional information is required, namely (i) the radius dependence of the melting temperature of Bi nanocrystals, $T_{\text{m}}(R)$; (ii) the radius and temperature dependences of the electron density of Bi nanoparticles in crystalline and liquid phases [$\rho_{\text{ec}}(T, R)$ and $\rho_{\text{el}}(T, R)$, respectively]; and (iii) the temperature dependence of the electron density of the glass matrix, $\rho_{\text{eg}}(T)$.

To account for the radius-dependent intrinsic stress contraction, the electron densities of Bi nanoparticles in both crystalline and liquid states were derived from the surface stress f, the Laplace–Young equation and the relation proposed by Liang and co-workers (Jiang *et al.*, 2001; Liang *et al.*, 2003) (Section 2.2) in which the liquid–solid interface energy is determined from the thermodynamic properties of bulk Bi. In the particular case of Bi, it was shown that the nanoparticles are not wetted by the sodium borate glass, so the interface energies are expected to be approximately the same as the surface energies of liquid and crystalline Bi (Liang *et al.*, 2003). Relevant values related to the liquid and crystalline phases of bulk Bi and sodium borate glass are reported in Table 2.

Table 3
Coefficients of thermal expansion β, specific mass ρ_0 and melting temperature T_{m} of bulk Bi determined from the best fit of equation (1) to the experimental SAXS intensity by applying equation (18) for describing the radius dependence of the melting temperature and equations given in Section 2.2.

Sample	$\beta_{\text{liquid Bi}}$ (K^{-1})	$\beta_{\text{crystal Bi}}$ (K^{-1})	$\rho_{0\ \text{liquid Bi}}$ at 544.52 K (kg m^{-3})	$\rho_{0\ \text{crystal Bi}}$ at 297 K (kg m^{-3})	$T_{\text{m}}(R \rightarrow \infty)$ (K)
A	8×10^{-5}	4×10^{-5}	10040	9844	535
B	7×10^{-5}	4×10^{-5}	9990	9844	535
C	4×10^{-5}	4×10^{-5}	10020	9844	535
Bulk Bi	1.21×10^{-4}	4.02×10^{-5}	10050	9747	544.52

Equation (18) was used in this study to describe the radius dependence of the melting temperature of Bi nanocrystals. The experimental $I(q, T)$ functions corresponding to different q values are plotted in Fig. 2 (blue symbols). In addition, the size-dependent compressive stresses on both crystalline and liquid Bi nanoparticles were calculated according to the theory described in Section 2.2 using the Bi bulk values of κ, S_{vib}, H_{m}, V_{mol} and γ_{vl} given in Table 2. The specific masses and thermal expansion coefficients of the crystalline and liquid phases and the melting temperature of bulk Bi were determined from the best fitting of equation (1) to the experimental I versus T curves. As shown in Fig. 2, good agreements between experimental (blue symbols) and calculated SAXS intensity (solid lines) using the available data of bulk Bi were achieved, over a wide range of q values for which the SAXS intensity decreases by about one order of magnitude. On the other hand, for very small q values (not shown in Fig. 2) the experimental values of the SAXS intensity are somewhat larger than the values calculated using equation (1). This behavior can be attributed to the existence of a small population of much larger nanocrystals, thus leading to a minor contribution to the SAXS intensity in this q range of the scattering curve. Owing to the strong noise in the SAXS intensity curves $I(q)$ at high q values, the I versus T curves were displayed for different q values only up to a maximum q for which the noise in the I versus T curves was considered not too high.

Table 3 reports the melting temperature of crystalline bulk Bi determined from the best fit of equation (1) to the experimental SAXS intensity. Equation (18) was used to describe the radius dependence of the melting temperature, and the equations given in Section 2.2 were applied for determining the temperature dependences of the specific masses and the intrinsic size-dependent contraction. The final best-fitting procedure yielded reasonable agreement between the experimental and calculated I versus T curves. On the other hand, our analysis demonstrates that the values of the thermal expansion coefficients of liquid Bi nanodroplets determined from the best-fitting procedure (Table 3) are much smaller than those of bulk liquid Bi (Table 2). Table 3 also

reports the specific masses of liquid and crystalline bulk Bi at 544.52 and 297 K, respectively, which were likewise determined by best fitting equation (1).

In addition to the mentioned size-dependent stress, Bi nanocrystals are expected to be subject to an additional stress. Note that Bi nanoparticles during their previous formation and growth at higher temperatures are in the liquid state. As the specific mass of Bi in the liquid state is larger than that in the crystalline state, the volumes of the Bi nanoparticles increase upon crystallization, thus exceeding the volumes of the glass cavities in which the liquid nanodroplets were formed. This effect may explain the slightly high value of the specific mass of the crystalline phase derived from our analysis for bulk Bi, which is 1% higher than the value reported in the literature.

Moreover, since the coefficient of thermal expansion of crystalline Bi is higher than the thermal coefficient of the glass matrix, the compressive stress on the crystalline Bi nanoparticles increases during heating from room temperature up to the melting temperature. Previous studies showed that at 500 K the volume of crystalline Bi exceeds the volume of the cavity in the glass in which the particle is formed by 1.8% (Degenhardt *et al.*, 2017). This implies that the existence of an additional compressive stress on confined Bi nanocrystals produced by the glass matrix is *a priori* expected. This also explains why the specific masses of crystalline Bi nanoparticles determined from our best-fitting procedure (Table 3) are for all samples larger than the specific mass of crystalline bulk Bi under atmospheric pressure.

On the other hand, the coefficient of volume expansion of liquid bulk Bi is much larger than the coefficient of sodium borate glass (Table 2). As a consequence, during cooling from the temperature at which droplets are formed down to room temperature, the volumes of the Bi nanodroplets become progressively smaller than the volumes of the cavities in the glass matrix in which they formed. Therefore, no compressive stress on the confined Bi nanodroplets is expected to occur. For this reason, the specific masses of liquid bulk Bi derived from our analysis are very close to those reported in the literature, the relative difference being from 0.1 to 0.6% (Lide, 1997).

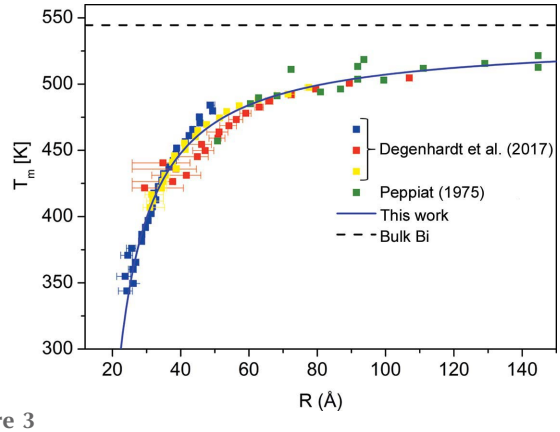

Figure 3
Solid line: melting temperature of spherical Bi nanocrystals as a function of their radius determined by applying the procedure described in the text. Symbols: several experimentally determined sets of radius-dependent melting temperatures of Bi nanocrystals reported in the literature (Degenhardt *et al.*, 2017; Peppiat, 1975).

The melting temperature of bulk Bi determined in this study is about 10 K lower than the melting temperature reported for bulk Bi at atmospheric pressure. The observed decrease in the melting temperature of Bi nanocrystals as compared to that of bulk Bi can be explained by the already mentioned compressive stress exerted by the glass matrix, which is a consequence of the fact that the specific mass of Bi nanocrystals obtained from our modeling is higher than the specific mass of Bi nanocrystals at atmospheric pressure. For a compressive stress causing a decrease of 1.8% in the volume of the crystalline phase of Bi, the Clausius–Clapeyron equation predicts a depression in melting temperature equal to 10.6 K (Degenhardt *et al.*, 2017). Under this condition our results indicate that the melting temperature of stress-free bulk Bi would be 535.52 K, in good agreement with the value 535 K determined from our best-fitting procedure.

The melting temperature T_m was determined as a function of the radius R by applying equation (18) using the best known value of S_{vib} for Bi (3.78 J mol^{-1} K^{-1}) (Regel & Glazov, 1995) and a value $h = 4.75$ Å ($R_0 = 3h$) derived from the best fitting of equation (1) to the experimental SAXS intensity. The same values of S_{vib} and h were used for the analyses of SAXS data of all investigated samples. Fig. 3 shows as a solid line the calculated melting temperature of Bi nanocrystals as a function of their radius, together with several sets of experimental results reported in the literature (Degenhardt *et al.*, 2017; Regel & Glazov, 1995). The good agreement of the calculated $T_m(R)$ function with previous experimental data confirms the good sensitivity of the SAXS intensity to the changes in volume and specific masses of nanoparticles on melting.

The good agreement of the modeled $T_m(R)$ function and experimental results shown in Fig. 3 suggests that the proposed procedure actually is an accurate method for determination of the radius dependence of the melting temperature of spherical nanocrystals as well as for the determination of thermal expansion coefficients and specific masses of confined nanoparticles. The results plotted in Fig. 3 imply that Bi nanoparticles in sodium borate glass with a radius lower than 22 Å at 297 K (near room temperature) are in the liquid state, this temperature being almost 250 K lower than the melting temperature of bulk crystalline Bi.

Note that a similar procedure could be applied to investigate the crystallization transitions of amorphous nanoparticles in solid matrices. Moreover, provided the specific masses of the solid and liquid phases are different, the proposed procedure – using only SAXS data – can also be applied to studies of phase transitions of noncrystalline nanoparticles for which X-ray or electron diffraction cannot usually be applied.

5. Conclusions

A novel procedure was developed for the determination of the radius dependence of the melting temperature of spherical nanocrystals in dilute solution embedded in a homogeneous

matrix. This procedure only uses data derived from SAXS measurements corresponding to dilute solutions of size-polydisperse spherical nanocrystals in solid matrices. The proposed method is based on the sensitivity of the SAXS technique to small but not negligible changes in size and electron density upon nanoparticle melting.

The proposed procedure was applied to determining the radius dependence of the melting temperature of polydisperse sets of Bi nanocrystals embedded in a sodium borate glass in dilute solution. The calculated function relating the melting temperature with nanocrystal radius is in remarkably good agreement with previous experimental results reported in the literature.

This investigation also demonstrated that Bi nanocrystals are subject to a size-dependent compressive stress and to an additional compressive stress produced by the glass matrix. This additional stress is a consequence of the increase in nanoparticle volume upon crystallization and differences between the thermal expansion coefficient of Bi nanocrystals and that of the glass in which they are embedded.

The procedure applied here to determine the melting temperature of Bi nanocrystals as a function of their radius can also be applied to determine other relevant parameters and properties, such as specific masses, thermal expansion coefficients of crystalline and liquid nanoparticles, vibrational entropy, and solid/liquid interface energies.

The novel procedure proposed in this article can also be applied to the determination of the radius dependence of melting and crystallization temperatures of amorphous nanoparticles. Since the SAXS technique is sensitive to changes in density and volume of nanoparticles – irrespective of their internal atomic arrangement – the proposed procedure is also useful for investigations of phase transitions of noncrystalline nanoparticles for which other techniques currently applied, such as X-ray and electron diffraction, do not yield useful information.

Funding information

The following funding is acknowledged: CNPq (grant Nos. 307133/2014-1 and 420781/2016-1).

References

Aqra, F. & Ayyad, A. (2011). *Mater. Lett.* **65**, 760–762.
Archer, D. G. (2004). *J. Chem. Eng. Data*, **49**, 1364–1367.
Bobkova, N. M. (2003). *Glass Phys. Chem.* **29**, 501–507.
Couchman, P. R. & Jesser, W. A. (1977). *Nature*, **269**, 481–483.
Degenhardt, H. F., Kellermann, G. & Craievich, A. F. (2017). *J. Appl. Cryst.* **50**, 1590–1600.
Dick, K., Dhanasekaran, T., Zhang, Z. & Meisel, D. (2002). *J. Am. Chem. Soc.* **124**, 2312–2317.
Emsley, J. (1991). *Elements*, 2nd ed. New York: Oxford University Press.
Freitas, J. C. C., Nunes, E., Passamani, E. C., Larica, C., Kellermann, G. & Craievich, A. F. (2006). *Acta Mater.* **54**, 5095–5102.
Garrigos, R., Kofman, R., Cheyssac, P. & Perrin, M. Y. (1986). *Europhys. Lett.* **1**, 355–360.
Goldstein, A. N., Echer, C. M. & Alivisatos, A. P. (1992). *Science*, **256**, 1425–1427.
Haro-Poniatowski, E., Serna, R., Suárez-García, A. & Afonso, C. N. (2005). *Nanotechnology*, **16**, 3142–3145.
Jiang, Q., Liang, L. H. & Zhao, D. S. (2001). *J. Phys. Chem. B*, **105**, 6275–6277.
Jiang, Q., Zhang, Z. & Li, J. C. (2000). *Acta Mater.* **48**, 4791–4795.
Jo, Y. H., Jung, I., Choi, C. S., Kim, I. & Lee, H. M. (2011). *Nanotechnology*, **22**, 225701.
Kellermann, G. & Craievich, A. F. (2002). *Phys. Rev. B*, **65**, 134204.
Kellermann, G. & Craievich, A. F. (2003). *Phys. Rev. B*, **67**, 085405.
Kellermann, G. & Craievich, A. F. (2008). *Phys. Rev. B*, **78**, 054106.
Kellermann, G., Craievich, A. F., Neuenschwander, R. & Plivelic, T. S. (2003). *Nucl. Instrum. Methods Phys. Res. B*, **199**, 112–116.
Kellermann, G., Gorgeski, A., Craievich, A. F. & Montoro, L. A. (2015). *J. Appl. Cryst.* **48**, 520–527.
Kittel, C. (2005). *Introduction to Solid State Physics*, 8th ed. Hoboken: John Wiley & Sons.
Kofman, R., Cheyssac, P. & Garrigos, R. (1990). *Phase Transit.* **24–26**, 283–342.
Li, Y., Zang, L., Jacobs, D. L., Zhao, J., Yue, X. & Wang, C. (2017). *Nat. Commun.* **8**, 14462.
Liang, L. H., Li, J. C. & Jiang, Q. (2003). *Physica B*, **334**, 49–53.
Lide, D. R. (1997). *CRC Handbook of Chemisry and Physics*, 78th ed. Boca Raton: CRC Press.
Liu, M. & Wang, R. Y. (2015). *Sci. Rep.* **5**, 16353.
Lučić Lavčević, M. & Ogorelec, Z. (2003). *Mater. Lett.* **57**, 4134–4139.
Mays, C. W., Vermaak, J. S. & Kuhlmann-Wilsdorf, D. (1968). *Surf. Sci.* **12**, 134–140.
Mei, Q. S. & Lu, K. (2007). *Prog. Mater. Sci.* **52**, 1175–1262.
Muller, H., Opitz, Ch., Strickert, K. & Skala, L. (1987). *Z. Phys. Chem. Leipzig*, **268**, 634.
Peppiat, S. J. (1975). *Proc. R. Soc. London Ser. A*, **345**, 401–412.
Regel, A. R. & Glazov, V. M. (1995). *Semiconductors*, **29**, 405.
Sheng, H., Ren, G., Peng, L.-M., Hu, Z. & Lu, K. (1997). *J. Mater. Res.* **12**, 119–123.
Shi, F. G. (1994). *J. Mater. Res.* **9**, 1307–1314.
Sobolev, V. (2010). *Database of Thermophysical Properties of Liquid Metal Coolants for Gen-IV*. Mol: Belgian Nuclear Research Centre SCK-CEN.
Thomson, J. J. (1988). *Application of Dynamics to Physics and Chemistry*. London: MacMillan.
Vanfleet, R. R. & Mochel, J. M. (1995). *Surf. Sci.* **341**, 40–50.
Wang, H. & Zhu, H. (2015). *Nanoscale Res. Lett.* **10**, 487.
Wasserman, H. J. & Vermaak, J. S. (1972). *Surf. Sci.* **32**, 168–174.
Wronski, C. R. M. (1967). *Br. J. Appl. Phys.* **18**, 1731–1737.
Xu, Q., Sharp, I. D., Yuan, C. W., Yi, D. O., Liao, C. Y., Glaeser, A. M., Minor, A. M., Beeman, J. W., Ridgway, M. C., Kluth, P., Ager, J. W. III, Chrzan, D. C. & Haller, E. E. (2007). *Phys. Rev. Lett.* **99**, 079602.
Yu, X. F., Liu, X., Zhang, K. & Hu, Z. Q. (1999). *J. Phys. Condens. Matter*, **11**, 937–944.